Dependences of the Optical Absorption, Ground State Energy Level, and Interfacial Electron Transfer Dynamics on the Size of CdSe Quantum Dots Adsorbed on the (001), (110), and (111) Surfaces of Single Crystal Rutile TiO_2

Taro Toyoda,[*,†,‡] *Qing Shen,*[*,†,‡] *Keita Kamiyama,*[§] *Kenji Katayama,*[#] *and Shuzi Hayase,*[//,‡]

[†]Department of Engineering Science, The University of Electro-Communications, 1-5-1 Chofugaoka, Chofu, Tokyo 182-8585, Japan

[§]Bunkoukeiki Co., Ltd, 4-8 Takakura, Hachioji, Tokyo 192-0033, Japan

[#]Department of Applied Chemistry, Chuo University, 1-13-27 Kasuga, Bunkyo, Tokyo 112-8551, Japan

[//]Graduate School of Life Science and Systems Engineering, Kyushu Institute of Technology, 2-4 Hibikino, Wakamatsu-ku, Kitakyushu, Fukuoka 808-0196, Japan

[‡]Core Research for Evolutional Science and Technology (CREST), Japan Science and Technology Agency (JST), 4-1-8 Honcho, Kawaguchi, Saitama 332-0012, Japan

ABSTRACT: Quantum dots (QDs) provide an attractive alternative sensitizer to organic dyes. However, there have been few reports on quantum dot-sensitized solar cells (QDSCs) that have photovoltaic conversion efficiencies exceeding those of dye-sensitized solar cells. This is because of the lack of fundamental studies of QDs on conventional nanocrystalline metal oxide electrodes. An important first step is an investigation of the dependences of the optical absorption, the ground state energy level, and the interfacial electron transfer (IET) on the size of QDs deposited on well characterized single crystal oxides. The present study focuses on a system of CdSe QDs adsorbed on the (001), (110), and (111) surfaces of single crystal rutile-TiO_2. The optical absorption spectra, characterized using photoacoustic spectroscopy, were found to be independent of the surface orientation. However, the exponential optical absorption tail (Urbach tail) suggests that the disorder decreases with the increasing size of the QDs, and is related to the surface orientation. The ground state energy levels of the QDs were characterized using photoelectron yield spectroscopy. Those on (001) and (111) surfaces show an upward shift as the size of QDs increases, while that on the (110) surface shows a downward shift, indicating a difference between the pinning effects for the different surface orientations. The IET rate constant and the relaxation component were characterized using the transient grating method. The IET rate constant was found to decrease as the size of the QDs increases and depends on the surface orientation, indicating differences in the decrease of the free energy change. The relaxation component increases with increasing QD size and depends on the surface orientation. This correlates with the density of states in the conduction band of rutile-TiO_2.

KEYWORDS: semiconductor quantum dot, TiO_2 single crystal, photo-sensitization, ionization energy, interfacial electron transfer, photoacoustic spectroscopy, photoelectron yield spectroscopy, transient grating method,

INTRODUCTION

When the size of a semiconductor material is reduced to dimensions below its effective exciton Bohr radius, exciton confinement results in the evolution of discrete optical transitions that gradually shift to higher energies with decreasing size (quantum confinement effect). Controlling the dimensions of semiconductor materials at the nanoscale level (thus creating quantum dots, QDs) is a promising strategy for developing novel functionality for various applications, including solar cells (quantum dot-sensitized solar cells, QDSCs).[1-15] Thus, the most appealing quality of QDs from both academic and industrial perspectives is their size-dependent electronic properties. Due to the size-dependent quantum confinement effect, QDs have a tunable energy gap between the ground and excited states, and higher extinction coefficients, which suggests the possibility of using them as sensitizers in place of dyes. Moreover, the electron injection process benefits from the large built-in dipole moments produced in the QDs that facilitate the separation processes of the electron-hole pairs.[16,17] These characteristics of QDs provide them with the possibility of boosting the light-to-energy conversion efficiency of QDSCs. In the quest for higher light-to-electric conversion efficiencies and lower production costs, a number of researchers have proposed QDSC architectures stretching over two decades where nanoparticles of wide bandgap semiconductors are photosensitized with QDs. Although QDs have such advantages, there have been few reports on QDSCs with photovoltaic conversion efficiencies equaling or exceeding those of dye-sensitized solar cells (~ 12%).[18] This is because of the lack of fundamental studies of the electronic structure and the interfacial electron transfer (IET) of QDs adsorbed on nanocrystalline metal oxide electrodes. In general, nanoparticulate TiO_2 electrodes play a key role in applications to QDSCs, because they offer a large surface area onto which a large amount of QDs can be adsorbed for light harvesting.[19] For QDs adsorbed on TiO_2 and other metal oxide nanoparticulate

electrodes, heterogeneity can be caused by the distributions of defects, adsorption sites, and the exposed surfaces on the oxide. Also, the heterogeneity can be caused by distributions in the parameters of the QDs, such as their size, shape and charge, as well as their interactions.[20] These complexities cloud a detailed understanding of the essential factors that contribute to the electronic structure and IET of QDs adsorbed on nanoparticulate TiO_2 electrodes.

In a fundamental study, it is important and necessary to investigate the dependencies of the optical absorption, the ground state energy level, and the IET processes on the size of the QDs on well characterized single crystal metal oxide surfaces, where the electronic structure has been well investigated.[20,21] Nevertheless, a detailed study of the influence of electrodes with different crystal orientations is seldom discussed except in a few reports. A high photovoltaic conversion efficiency (~ 4.73%) for PbS QD heterojunction solar cells using anatase (001) TiO_2 nanosheet electrodes has been reported.[22] The better photovoltaic performance of the nanosheet compared to nanoparticles may be attributed to the high reactivity of the (001) surface owing to the higher ionic charge of this surface compared to the thermodynamically stable (101) surface.[23] Maitani and co-workers have revealed the effect of the reactive {001} facet on the photoexcited charge transfer from organic fluorophores to anatase-TiO_2 nanoparticles. The results imply a significant enhancement of the photoexcited charge transfer from fluorophores to TiO_2 nanoparticles due to the reactive {001} facet with a maximum factor of more than 10 in the quenching rate constant.[24] Parkinson and co-workers have used dyes and several QDs to sensitize single crystal surfaces to create a simple model for studying the basic processes related to IET in single crystal metal oxide electrodes.[25-32] The function of QDSCs relies on IET from the QD to a large band gap metal oxide (MO) (TiO_2, ZnO etc.) and it is the first important step for solar cell performance. Although the effects on IET of the size of QDs and the QD-MO spacing have been studied for various materials,

the previous studies of the IET from molecules and QDs to nanoparticulate TiO_2 electrodes have revealed highly heterogeneous IET dynamics because of the heterogeneity and polycrystalline nature of nanoparticulate TiO_2.[32-42] Recently, the IET rate of CdSe QDs on rutile-TiO_2 (R-TiO_2) electrodes with different crystal orientations has been studied as a function of the energy gap (ΔE) between the conduction band minimum of R-TiO_2 and the first excited state of the CdSe QDs.[43] The IET rate constant of CdSe QDs on a (111) surface with respect to ΔE is higher than those on the (001) and (110) surfaces, indicating differences in the crystal binding and the mixing of wave functions at the interface.[43]

The present study focuses on the QD size-dependencies of the optical absorption, the ground state energy, the IET rate constant, and the components of the IET in systems comprising CdSe QDs on single crystal R-TiO_2. We chose CdSe QDs as the sensitizer as these are the most extensively studied. Knowledge of the QD size-dependencies of the optical absorption, ground state energy, and IET is important in order to clarify the nature of the interaction between the QDs and R-TiO_2. We chose single crystal R-TiO_2, which is not only ideal for studying the crystal growth of the QDs but is also useful for studying the interactions between the QDs and TiO_2. The rutile phase is the most stable and has been the subject of most fundamental studies because of the ready access to large bulk single crystals and relatively easy surface preparation procedures.[21] First, we applied photoacoustic (PA) spectroscopy, which is a type of photothermal spectroscopy, to characterize the optical absorption, not only in the bandgap absorption region but also in the sub bandgap region.[15,44,45] The PA signal is less sensitive to light-scattering effects than the signals in conventional spectroscopy. The sensitivity is higher for weak absorption than that of the conventional technique. Second, we applied photoelectron yield (PY) spectroscopy.[46,47] Although PY spectroscopy has been used to determine the ionization energy of a number of bulk

semiconductors and metals, it has not been applied to the study of the ionization energy of QDs as a function of size. While UV optical absorption spectra specify the energies of bands relative to each other and give information only at the band edge, they do not determine the absolute energy levels. Understanding of the absolute energy levels is vital in order to get a complete picture of the electronic structure, including the quantum confinement effect in the system. PY spectroscopy is useful for determining the absolute ground state energy level of CdSe QDs on R-TiO_2, in contrast to ultraviolet visible (UV) spectra. Advantageously, the PY method is a rapid and reproducible measurement that can be done under ambient conditions.[46,47] Third, we applied the improved-transient grating (TG) method to characterize the IET dynamics.[14] Basically, the TG method depends on the refractive index changes resulting from photoexcited carriers. In this method, a diffraction grating consisting of photoinduced charge carriers was utilized for monitoring the carrier dynamics. The improved-TG method features very simple optical alignment, high sensitivity, and evaluation of both the electron and hole relaxation processes, under low pump light intensity.[14,48,49] Comparison of the IET dynamics for IET from CdSe QDs to single crystal R-TiO_2 with different crystal surfaces as a function of the size of the QDs leads to an understanding of the charge injection dynamics and suggests possible ways to improve QDSCs.

EXPERIMENTAL SECTION

Materials and Chemicals. The characteristics of single crystal R-TiO_2 have already been reported.[50] Single-crystal R-TiO_2 wafers, 5 mm x 7 mm in area and 0.5 mm thick, with (001)-, (110)-, and (111)-cuts were obtained from Furuuchi Chemical Co., Ltd., Japan. The surface roughness of the (001), (110), and (111) surfaces were 0.322 nm, 0.356 nm, and 0.394 nm,

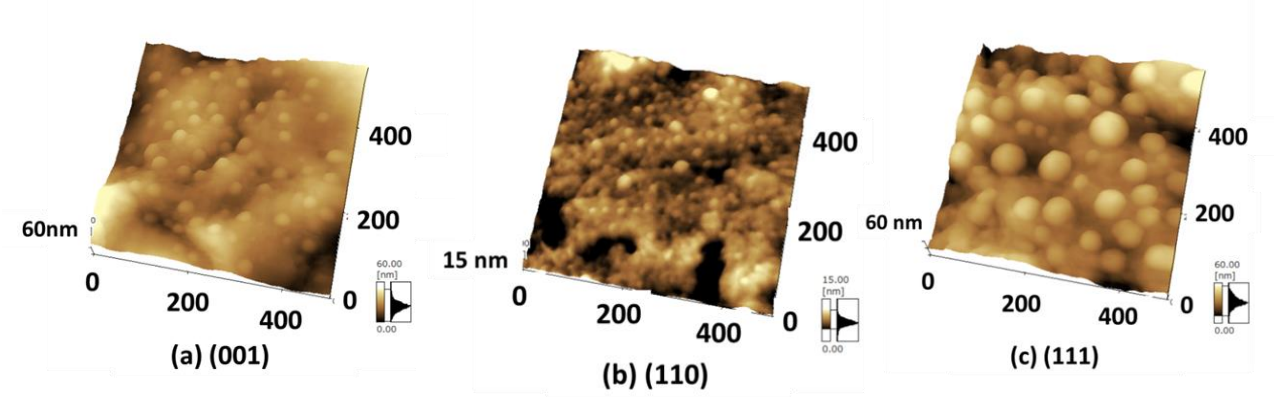

Figure 1. AFM images of CdSe quantum dots adsorbed on the (a) (001), (b) (110), and (c) (111) surfaces of single crystal of R-TiO_2 (adsorption temperature 10°C; adsorption time, 4 h).

respectively. The flat surfaces were treated by washing them in acetone for 30 min, immersing them in distilled water for 30 min, and exposing them to ozone for 10 min. CdSe QDs were adsorbed on the surfaces of the wafers using a chemical bath deposition (CBD) technique.[50] An 80 mM sodium selenosulphate (Na_2SeSO_3) solution was prepared by dissolving elemental Se powder in a 200 mM Na_2SO_3 solution. Then, 80 mM $CdSO_4$ and 120 mM of the trisodium salt of nitrilotriacetic acid [$N(CH_2COONa)_3$] were mixed with the Na_2SeSO_3 solution in a volume ratio of 1:1:1. The single crystal R-TiO_2 was placed in a glass container filled with the final solution at 10ºC in the dark for various times (4 ~ 28 h). Figure 1 shows examples of AFM images of CdSe QDs adsorbed on (a) (001) R-TiO_2, (b) (110) R-TiO_2, and (c) (111) R-TiO_2. The adsorption temperature and time were 10ºC and 4 h, respectively. The AFM images show that there are many more CdSe QDs on the (111) surface than on the (001) and (110) surfaces. Also, the rate of adsorption from optical absorbance measurements of the CdSe QDs on the (111) surface is higher than for those deposited on the (001) and (110) surfaces, similar to results previously reported ((111) > (110) > (001)).[50] Therefore, the adsorption of CdSe QDs on R-TiO_2 is related to the orientation of the surface and its associated electronic structure. Characterization of the crystal

structure of CdSe QDs by conventional XRD measurements was not possible due to the small number of QDs. One would like to characterize the structure by high-resolution XRD measurements, since the ground state energy level of the QDs might depend on the crystal structure.[51]

PA Spectroscopy Characterization. The optical absorption of CdSe QDs on R-TiO_2 were investigated using a single beam PA spectrometer with a gas-microphone technique.[15] The PA cell consists of an aluminum cylinder with a small channel at the periphery into which a microphone is inserted. Monochromatic light from a 300 W xenon short arc lamp modulated at 33 Hz was focused onto the sample surface in the sealed PA cell. The PA signal was detected by first passing the output from the microphone through a preamplifier and then a lock-in amplifier. The spectra were taken at room temperature in the wavelength range of 300 – 830 nm. The PA signal intensity is proportional to the optical absorption coefficient due to the relationship between the optical absorption length and the thermal diffusion length.[52] The spectra were calibrated using the PA signals from a carbon black sheet.[15,52]

PY Spectroscopy Characterization. The PY spectra were collected using an ionization energy measurement system (BIP-KV201, Bunkoukeiki, Co., Ltd., Japan).[15,43] The number of photoelectrons was obtained using an ammeter to measure the current needed to compensate for the photoexcited holes generated in the sample. In the PY measurements, the photoemission yield (Y) was measured as a function of photon energy (hv), and the value of the ionization energy (I) was determined from the onset of the PY spectrum. The PY spectrum around the photoelectric threshold I can be expressed by the following equation

$$Y = K\,(hv - I\,)^n \qquad (1)$$

where K is a constant and n is a parameter that mainly depends on the shape of the density of electronic states at the upper edge of the valence band and the probability of the transmission of electrons across the surface.[46] In this study, we employed a cubic function (n = 3) based on a theoretical analysis.[46,53] The value of I was determined by extrapolating the linear part of $Y^{1/3}$ to the baseline.[15] An energy scan of the incident photons was performed with UV light (4 ~ 9.5 eV). The UV light was focused on the sample over an area of 1 × 3 mm^2. All the measurements were performed in a vacuum chamber (~ 4 × 10^{-3} Pa) at room temperature.

Improved-TG Characterization. For these measurements, a laser beam was separated into two parts for the pump and probe beams. These were then aligned coaxially before being trained on the transmission grating. For the pump beam, the spatial intensity profile has an interference pattern close to the surface on the far side of the transmission grating. When a sample is brought near to this surface, it is excited by the optical interference pattern. The probe beam is diffracted both by the transmission grating and by the grating induced on the sample (TG). The two diffractions progress in the same direction and the time dependent diffraction intensity is measured.[14] The laser source used for this characterization was a regeneratively amplified titanium/sapphire laser (CPA-1000, Clark-MXR Inc., USA) with a fundamental wavelength of 775 nm, a repetition rate of 1 kHz, and a pulse width of 150 fs. The probe pulse (775 nm) was delayed by an optical delay line (0 ~ 400 ps). The pump pulse was generated using a travelling-wave optical parametric amplifier of a super fluorescence (TOPAS) system and was set at a wavelength of 500 nm, suitable for optical absorption in CdSe QDs. The diameters of both the pump and probe lasers were 5 mm. We have shown previously that the mechanism for carrier depopulation by the TG technique under our experimental conditions (2 ~ 7 μJ/pulse: linear response range) is due to hole trapping and electron injection or trapping.[14] In this case, we were able to separate charge

transfer/trapping from charge recombination, simplifying the data analysis. Also, samples exhibited no apparent photo-damage during the TG experiments.

RESULTS AND DISCUSSION

PA Characterization of CdSe QDs on Single Crystal R-TiO_2. Figure 2 (a) shows an example of the PA spectra for CdSe QDs on the (111) surface of single crystal R-TiO_2 with different adsorption times (12 ~ 24 h). The shapes of the PA spectra are independent of the modulation frequency (33 ~ 233 Hz) of the incident light, indicating reflection of the optical absorption coefficient character. Similar PA spectra can be obtained for CdSe QDs on the (001) and (110) surfaces of single crystal R-TiO_2. The energy gap between the ground and excited states (first excitation energy) was evaluated using the shoulder point (↓, energy value is E_1). In general, the values of E_1 in the logarithmic PA spectra agree well with the reported values of the bandgaps.[54] A redshift in E_1 with increasing adsorption time is perceptible, suggesting the growth of CdSe QDs. With the values of E_1 and the bandgap (E_g) for bulk CdSe, the average diameter, R, can be estimated from the effective mass approximation (EMA)[55] using the following equations

$$E_1 = E_g + \frac{h^2}{8\mu r^2} \tag{2}$$

$$\frac{1}{\mu} = \frac{1}{m_e^*} + \frac{1}{m_h^*}$$

where r is the radius ($R = 2r$) of the CdSe QDs, μ is the reduced mass, h is Planck's constant, m_e^* is the electron effective mass, and m_h^* is the hole effective mass. The Coulomb and correlation terms are neglected. Hence the EMA assumes an infinite potential barrier at the surface of the dot, and fails for small dot sizes because the bands at higher wave vectors are non-parabolic and

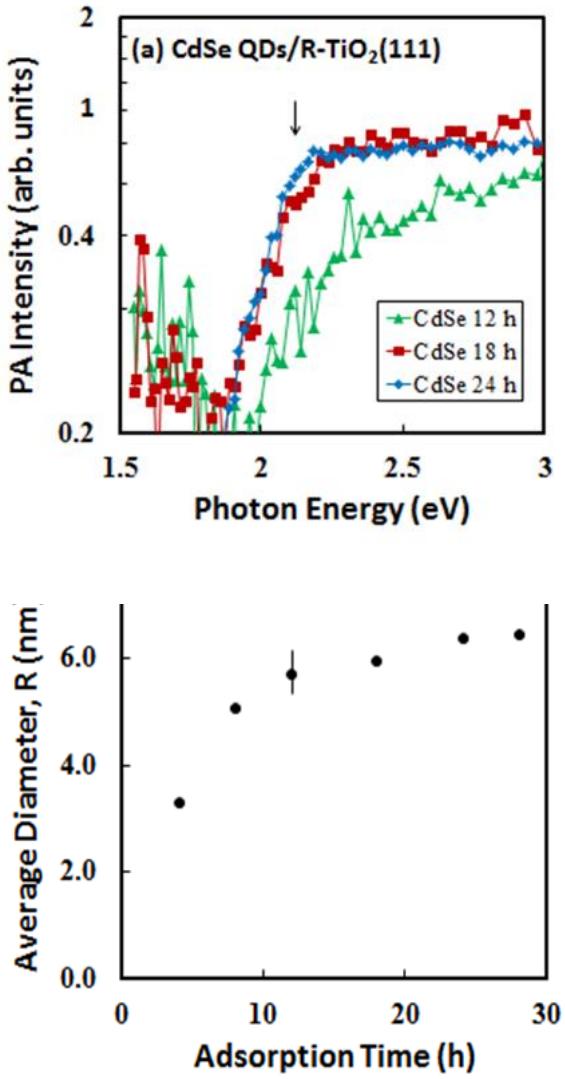

Figure 2. (a) Photoacoustic spectra for CdSe quantum dots adsorbed on the (111) surface of single crystal R-TiO_2. (b) Dependence of average diameter, *R*, on adsorption time.

the potential step at the surface of the dot is finite. Murray and co-workers showed that the size of CdSe QDs calculated by the EMA agree with the experimental results for CdSe QDs larger than 3 nm in diameter.[56] *R* values estimated from the PA measurements in our case were in the acceptable range of the EMA. Figure 2 (b) shows an example of the adsorption time dependence of *R* of CdSe QDs on the (111) single crystal R-TiO_2. *R* increases in diameter from 3.5 to 6.5 nm. Similar results were obtained for the other surfaces showing that the adsorption time dependence of *R* is

independent of the R-TiO_2 surface. However, the rate of adsorption measured by the optical absorbance in CdSe QDs on the (111) surface is higher than for those deposited on the (001) and (110) surfaces, giving a similar result to that reported previously ((111) > (110) > (001)).[50]

In semiconductors and insulators, the absorption edge in the region below the bandgap increases exponentially (Urbach tail or exponential tail).[57] The exact cause of the Urbach tail has been extensively studied.[58-63] One study gave fundamental information associated with the structural disorder, defects, impurities, and electron-phonon interactions.[62] The PA signal intensity (P) in the region of the Urbach tail is given by the following equation[62]

$$P = P_0 \exp\left[\frac{\sigma(h\nu - h\nu_0)}{k_B T}\right] \quad (3)$$

where h is Planck's constant ($h\nu$, incident photon energy), k_B is the Boltzmann constant, T is absolute temperature, and P_0 and ν_0 are fitting parameters. σ is a characteristic of the logarithmic slope (exponential tail) and is called the steepness parameter. Figure 3 (a), (b), and (c) show the dependence of the value of σ on R for CdSe QDs on (001), (110), and (111) single crystal R-TiO_2, respectively. We assume firstly that the value of σ is a reflection of the structural disorder from the ideal stoichiometry for CdSe QDs. Smaller σ corresponds to a broader exponential tail and hence to larger structural disorder.[64] The value of σ increases with increasing R, indicating a decrease in structural disorder. Another possibility for the R dependence of σ is the effect of electron-phonon interactions.[62] Our results suggest that the number of electron-phonon interactions is larger for smaller R because these interactions increase as the number of phonons at room temperature increases.[62] The structural disorder and electron-phonon interactions,

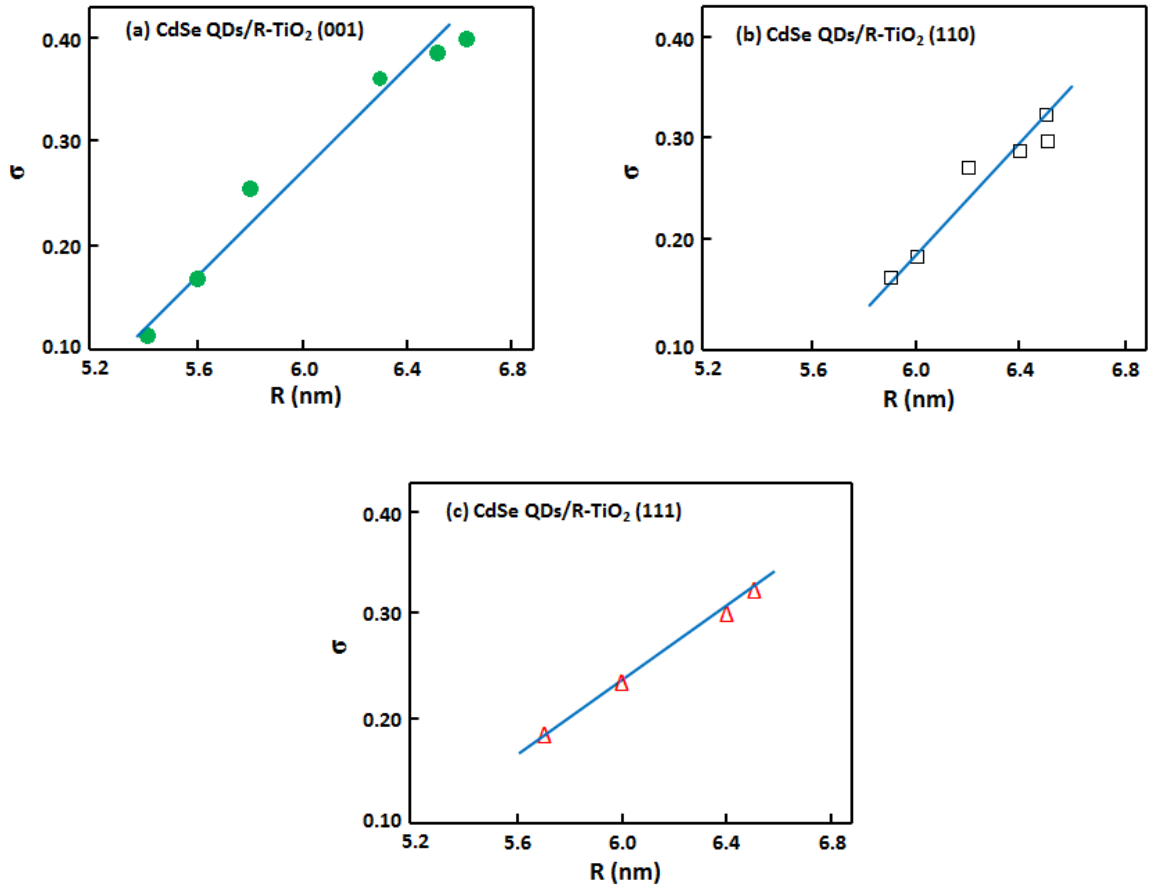

Figure 3. Dependence of steepness parameter, σ, on the average diameter, *R*, of CdSe quantum dots adsorbed on the (a) (001), (b) (110), and (c) (111) surfaces of single crystal R-TiO_2.

together with the impurities, strongly influence the optical absorption process.[59,62] The temperature dependence of σ is needed to account for the effects of the structural disorder and electron-phonon interactions for CdSe QDs on different electrode surface orientations.[62]

PY Characterization of CdSe QDs on Single Crystal R-TiO_2. The orientation of the crystal surface affects the ionization energy because the strength of the electric double layer at the surface is proportional to the density of positive ion cores. There is a double layer because the surface ions are asymmetric, with vacuum on one side and substrate on the other.[15] We utilized

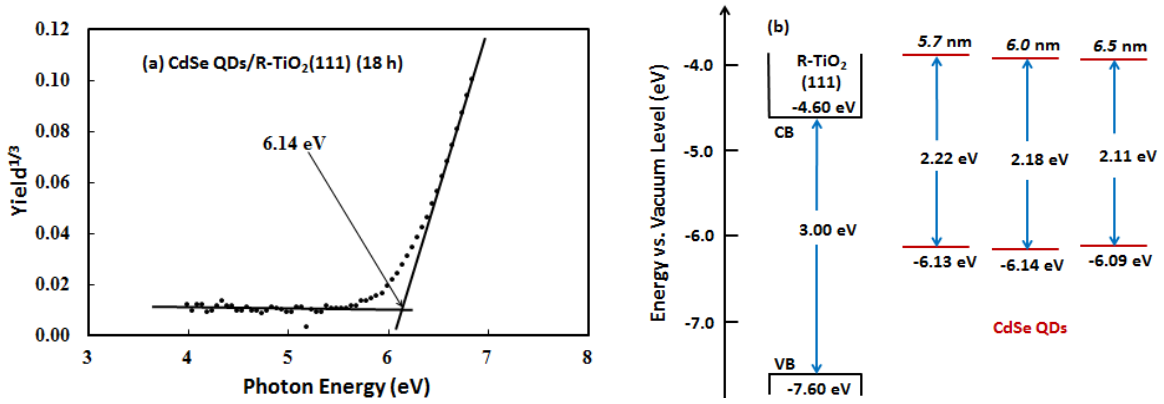

Figure 4. (a) Photoelectron yield spectrum of CdSe quantum dots adsorbed on the (111) surface of single crystal R-TiO_2. (b) alignment of energy levels.

the PY spectroscopy method to determine the size-dependent ground state energy level of CdSe QDs on (001), (110), and (111) single crystal R-TiO_2. Figure 4 (a) shows an example of the PY spectra of CdSe QDs grown on the (111) surface with an adsorption time of 18 h (~ 6 nm diameter). The error bars are included to show the good S/N ratio. Figure 4 (b) shows an example of the alignment of the energy levels of CdSe QDs on (111) R-TiO_2, together with the valence band maximum (VBM) positions of (111) R-TiO_2.[50,64] The positions of the VBM measured for (001), (110), and (111) R-TiO_2 were the same as reported previously (-7.83 eV, -7.74 eV, and -7.60 eV, respectively).[50] The size-dependent ground state and excited state energy levels of CdSe QDs on (a) (001), (b) (110), and (c) (111) single crystal R-TiO_2 are shown in Figure 5. Figure 5 shows that the ground state energy levels of CdSe QDs on the (001) and (111) surfaces shift upward with increasing R, while that on the (110) surface shifts downward. Here, the excited state energy levels of CdSe QDs on (001), (110), and (111) R-TiO_2 are evaluated from the PA characterization (E_1 value), and they show downward shifts with increasing R. In the simplest EMA model,[65] the ground and excited energy level shifts (ΔE_{GS} and ΔE_{ES},

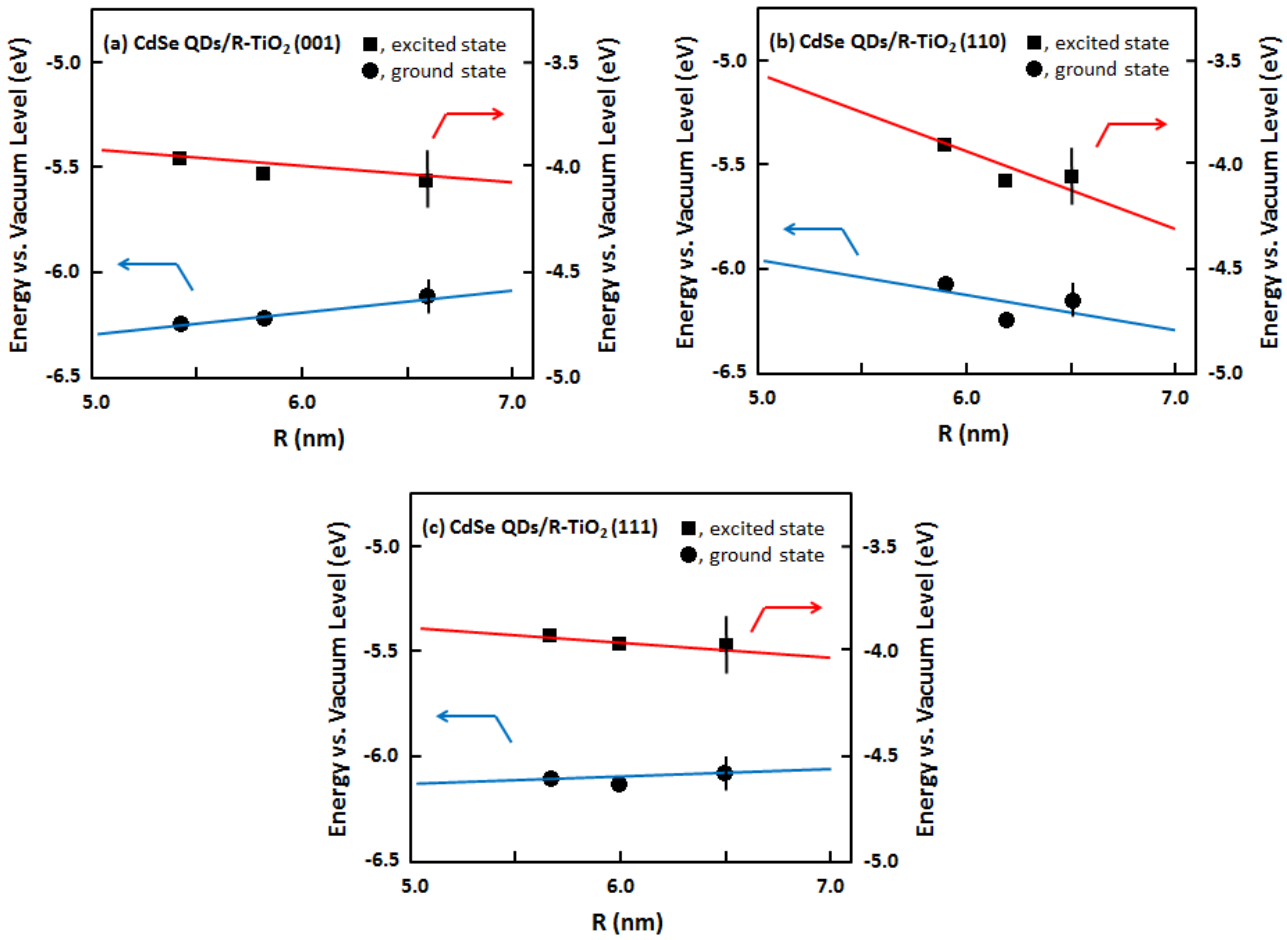

Figure 5. Dependence of ground state and excited state energy levels of CdSe quantum dots on average diameter, *R*, adsorbed on the (a) (001), (b) (110), and (c) (111) surfaces of single crystal R-TiO_2

respectively) are inversely proportional to the effective masses of the holes (m_h^*) and electrons (m_e^*), respectively, and given by

$$\Delta E_{GS} = \frac{-h^2}{2m_h^* R^2} \qquad \Delta E_{ES} = \frac{h^2}{2m_e^* R^2} \tag{4}$$

where *h* is Planck's constant, and *R* is the diameter of the QDs.[66] Since m_h^* for CdSe is three times heavier than m_e^*, EMA predicts the upward shift of the ground state energy level is approximately three times smaller than the downward shift of the excited state energy level. The measured

changes in ΔE_{GS} and ΔE_{ES} with R are smaller than those calculated from equation (4). This implies that EMA is inaccurate and overestimates the quantum confinement effect. There is a chemical interaction between the CdSe QDs and the R-TiO_2 surface upon adsorption that correlates with the ground states of the CdSe QDs. The interactions between CdSe QDs and the (001) and (111) R-TiO_2 surfaces are similar to each other because the R dependences of ΔE_{GS} and ΔE_{ES} are the same On the other hand, the interaction between CdSe QDs and the (110) R-TiO_2 surface is different because of the different R dependence of $\Delta E_{GS.}$ The different R dependence for the (110) surface is possibly due to the pinning of the CdSe QD ground state to the VBM of R-TiO_2, which is attributed to direct electronic interaction between the two semiconductor materials.[66]

TG Characterization of CdSe QDs on Single Crystal R-TiO_2. Figure 6 shows an example of the TG response for CdSe QDs grown on a R-TiO_2 (111) surface with an adsorption time of 18 h (~ 6 nm diameter). There are two relaxation processes: a fast one (~ 1 ps) and a slow one (several tens of ps). The TG signal intensity S(t) is proportional to the refractive index change, which is determined by a linear function of the concentration of free photogenerated carriers (electron and holes) according to the Drude model.[67,68] S(t) can be fitted with two exponential relaxation functions plus an offset (S_0)

$$S(\mathrm{t}) = A_1 \exp\left(\frac{-t}{\tau_1}\right) + A_2 \exp\left(\frac{-t}{\tau_2}\right) + S_0 \qquad (5)$$

where A_1, A_2, and S_0 are fitting parameters, which correspond to the components of the fast, slow, and longer relaxation processes, respectively. Here, we assume that S_0 is related to the recombination process. τ_1 and τ_2 are the time constants of the fast and slow relaxation processes, respectively. The two exponential functions together with the offset term fit with the

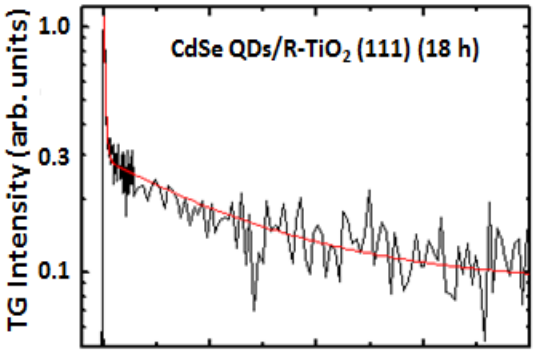

Figure 6. Transient grating response for CdSe quantum dots adsorbed on the (111) surface of single crystal R-TiO_2 (adsorption time, 18 h).

experimental data using a least-squares fit (red-line in Figure 6). The fast relaxation time constant τ_1 is observed to be around 1 ps. In the TG measurements, τ_1 is independent of the surface orientation. The fast relaxation process of around 1 ps region was not observed in the TG measurements when we characterized CdSe QDs adsorbed on a nanaoparticulate TiO_2 electrode.[49,67,68] We measured the TG responses of each single crystal rutile TiO_2 surface without CdSe QDs to investigate the effect of the TiO_2 only. In this case, similar fast relaxation processes with relaxation times of around 1 ps were observed for the three different surfaces. These TG responses are identical with those obtained for CdSe QDs on R-TiO_2. Therefore, the fast relaxation process is mainly due to the optical Kerr effect, which is an effect due to the electric field of the light itself. The optical Kerr effect causes a variation in the refractive index which is proportional to the local irradiation of the light. This effect is pronounced with intense beams such as lasers applied to single crystals. On the other hand, the fast relaxation processes in the region of several ps due to hole trapping[49,67,68] were not observed in our TG measurements on CdSe QDs on single crystal R-TiO_2 owing to the overlap of the TG signal intensity with the strong optical Kerr effect around 1 ps. Figure 7 shows the dependence on *R* of the relative value

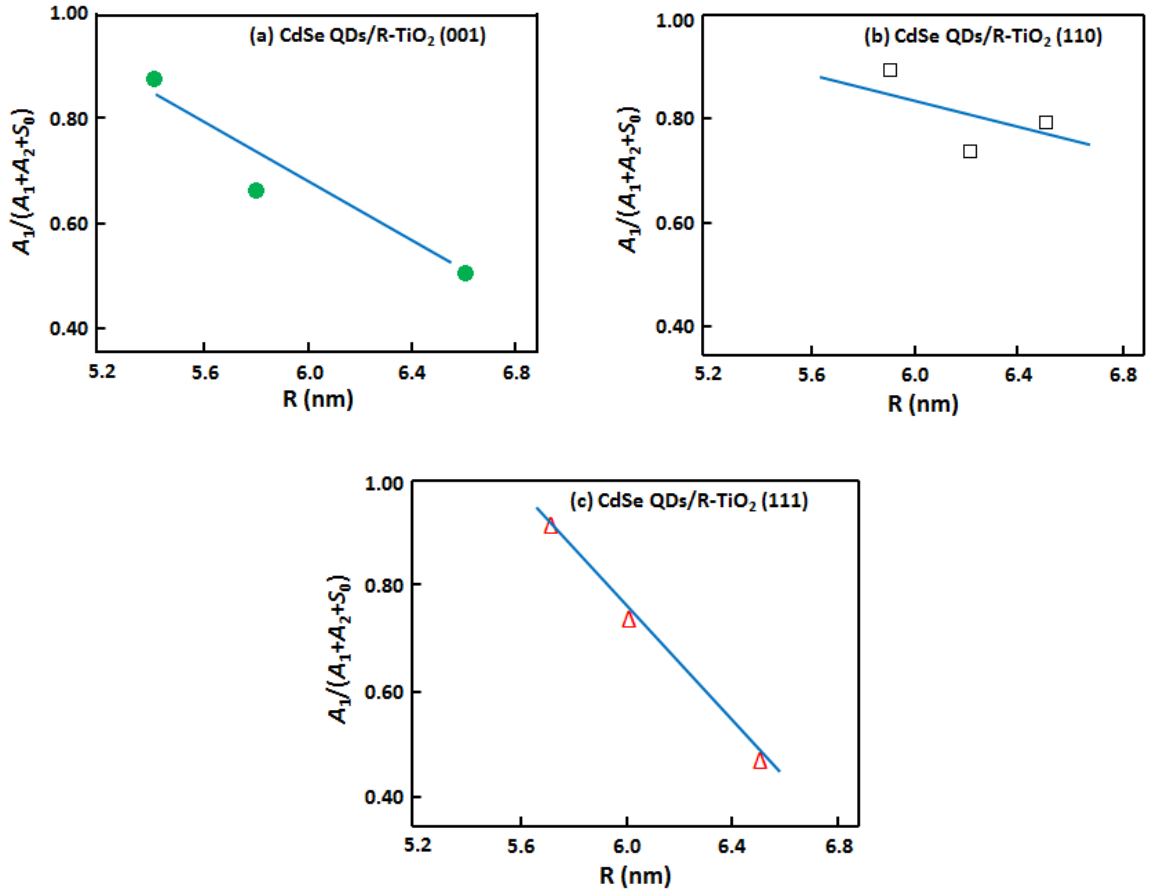

Figure 7. Dependence of the relative component of $A_1/(A_1 + A_2 + S_0)$ on the average diameter, R, of CdSe quantum dots adsorbed on the (a) (001), (b) (110), and (c) (111) surfaces of single crystal R-TiO_2.

of the parameter A_1 for the fast relaxation process to the value of the combined parameters ($A_1/(A_1 + A_2 + S_0)$) on (a) (001), (b) (110), and (c) (111) surfaces. The relative value depends on R and decreases with increasing R due to the decrease in penetration of the pump beam to the single crystal rutile TiO_2, corresponding to a decrease in the optical Kerr effect. However, the rate of decrease of the relative component of A_1 on the (110) surface is lower than those on the (001) and (111) surfaces, indicating a greater influence of the optical Kerr effect, despite the adsorption of QDs on the (110) surface being larger than that on the (001) surface. According to the PY characterization, the interactions between the CdSe QDs and R-TiO_2 for the (001) and (111)

surfaces are similar to each other. On the other hand, the interaction between the CdSe QDs and R-TiO_2 for the (110) surface is different. The different R dependence for the (110) surface is possibly due to pinning of CdSe QD ground state to the VBM of R-TiO_2, which is attributed to the direct electronic interaction between the two semiconductor materials.[66] The different pinning effect leads to the smaller ratio of the relative component of the relaxation process for the (110) surface.

The slow relaxation time constant τ_2 of between 30 and 80 ps is assumed to be due to the photoexcited electron relaxation process. τ_2 obtained in the measurements increases with increasing adsorption time similar to previous reports[37,68] and depends on the R-TiO_2 surface. We calculate the apparent IET rate constant, k_{et}, for CdSe QDs adsorbed on R-TiO_2 using the following relationship[69]

$$K_{et} = \frac{1}{\tau_2(TiO_2)} - \frac{1}{\tau_2\,(SiO_2)} \tag{6}$$

where $\tau_2\,(TiO_2)$ and $\tau_2\,(SiO_2)$ are the time constants of the QDs adsorbed on R-TiO_2 and SiO_2, respectively. Applying the time constant τ_2 in the measurements for QDs on R-TiO_2 and those on SiO_2 from the literature,[49] we calculated the apparent IET rate constant K_{et} using eq. (6). Figure 8 shows the dependence of K_{et} on R for QDs on (a) (001), (b) (110), and (c) (111) surfaces. K_{et} decreases with increasing R. This result can be explained by the fact that with larger R a smaller percentage of the total charge density is localized near the surface.[70] This causes a decrease in the free energy change, so that the IET rate constant decreases. The symmetry of the wave functions determines the total charge density.[70] The symmetry of the excited states of CdSe QDs to the orbitals of the substrate influences the IET rate constant. The rates of decrease of K_{et} for

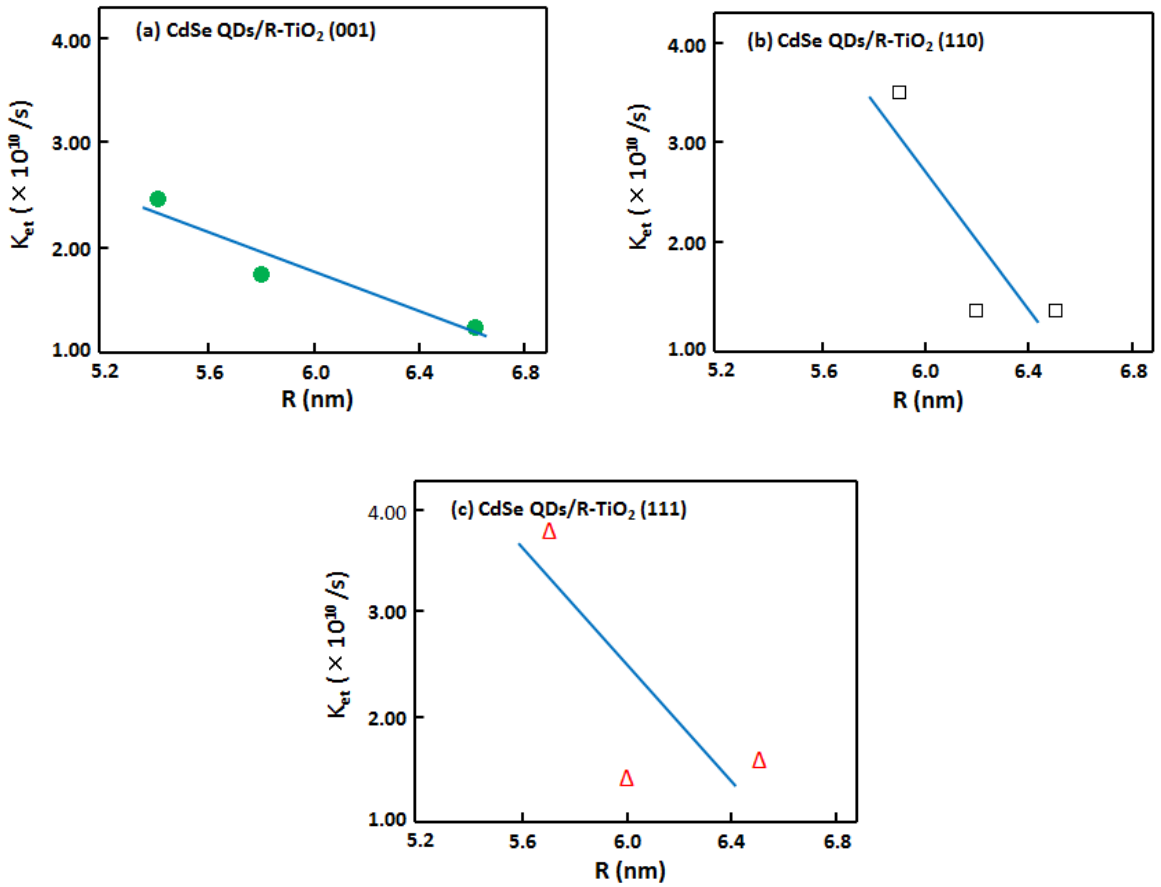

Figure 8. Dependence of the electron transfer rate constant, K_{et}, on the average diameter, R, of CdSe quantum dots adsorbed on the (a) (001), (b) (110), and (c) (111) surfaces of single crystal R-TiO_2.

the (110) and (111) surfaces are higher than that for the (001) surface, indicating that smaller percentages of the charge are localized near the (110) and (111) surfaces than near the (001) surface with increasing R. Figure 9 shows the dependence on R of the relative value of the parameter for the slow relaxation process ($A_2/(A_1 + A_2 + S_0)$) for QDs on (a) (001), (b) (110), and (c) (111) surfaces. The component A_2 depends on R and increases with increasing R. The rate at which A_2 increases for the (111) surface is higher than those for the (001) and (110) surfaces, indicating a difference in the density of states (DOS) in the conduction band for (111) R-TiO_2. The DOS of the conduction band of R-TiO_2 is dominated by Ti 3d orbitals. DFT calculations

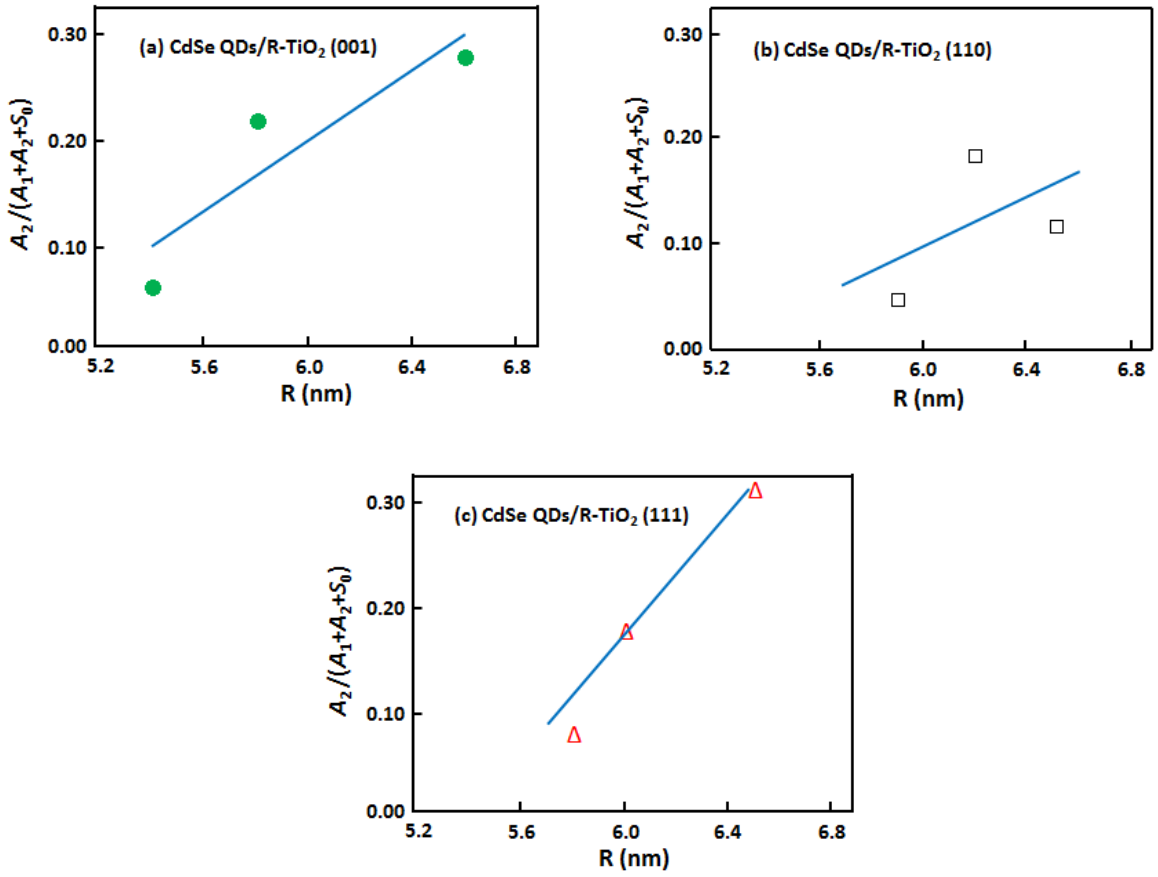

Figure 9. Dependence of the relative component of $A_2/(A_1 + A_2 + S_0)$ on the average diameter, R, of CdSe quantum dots adsorbed on the (a) (001), (b) (110), and (c) (111) surfaces of single crystal R-TiO_2.

have shown that the DOS due to Ti 3d orbitals for (001) and (110) R-TiO_2 is broad, between 1.6 and 6 eV. However, Ti 3d orbitals for (111) R-TiO_2 give rise to a somewhat narrower structure between 1.6 and 3.6 eV, suggesting the possibility of a higher DOS in (111) R-TiO_2 than the other crystal orientations.[43] Hence, there is a possibility that the higher rate of increase of $A_2/(A_1 + A_2 + S_0)$ with R in (111) R-TiO_2 is due to the higher DOS in (111) R-TiO_2. We have shown that (111) R-TiO_2 is suitable for the adsorption of CdSe QDs and electron transfer.[50,64] To clarify the effectiveness of (111) R-TiO_2 for sensitizing solar cells, we introduce the product of K_{et} and $A_2/(A_1 + A_2 + S_0)$. The value of $K_{et} \bullet A_2/(A_1 + A_2 + S_0)$ corresponds to the short circuit current

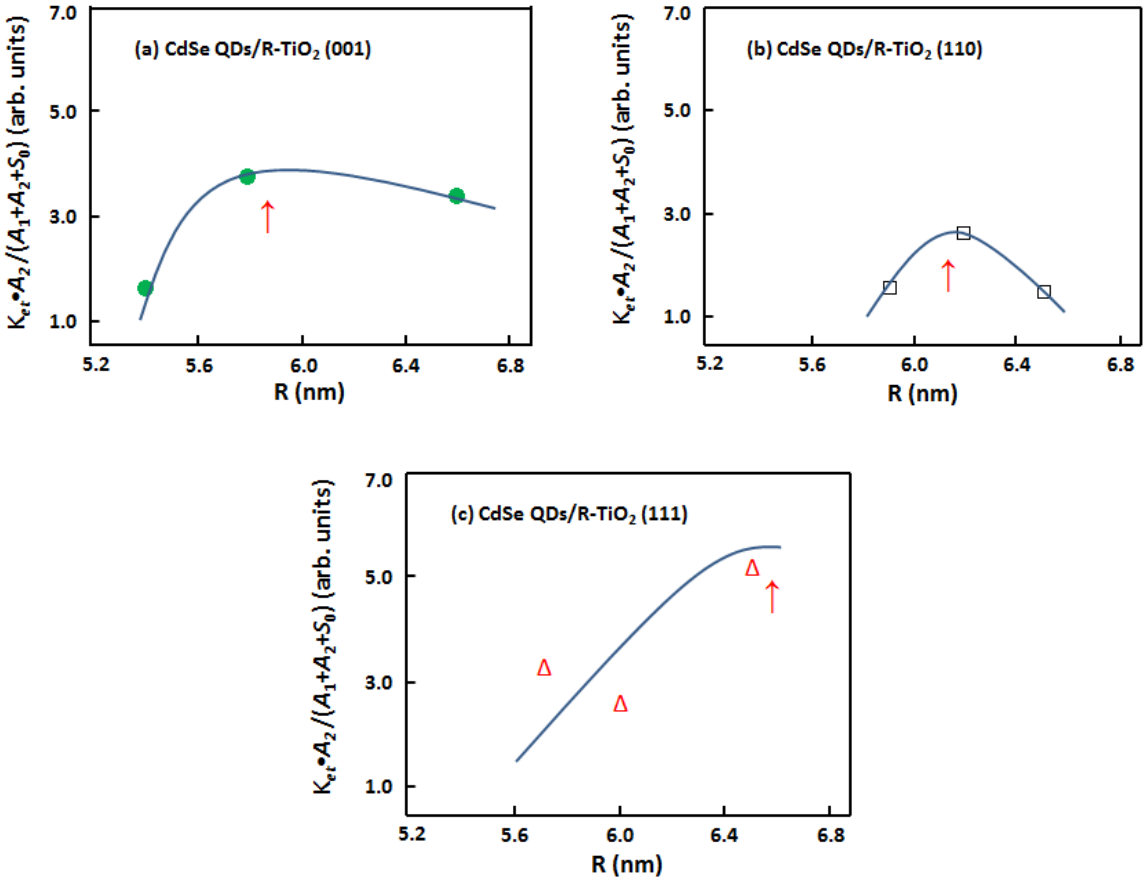

Figure 10. Dependence of the value of $K_{et} \bullet A_2/(A_1 + A_2 + S_0)$ on the average diameter, R, of CdSe quantum dots adsorbed on the (a) (001), (b) (110), and (c) (111) surfaces of single crystal R-TiO_2.

density, J_{sc}, in the photovoltaic cell. Figure 10 shows the dependence of $K_{et} \bullet A_2/(A_1 + A_2 + S_0)$ on R for the (a) (001), (b) (110), and (c) (111) surfaces. These each have maximum values. Figure 10 (c) shows that the maximum value on the (111) surface is higher than those on the (001) and (110) surfaces, indicating the effectiveness of (111) R-TiO_2 as a photoanode. Hence, the combination of a (111) R-TiO_2 nanosheet as a photoanode with CdSe QDs with diameters of ~ 6.6 nm can contribute to better photovoltaic performance of CdSe QDSCs, similar to the improvements achieved by applying photoelectrodes of anatase TiO_2 nanosheets with exposed (001) facets.[22]

CONCLUSIONS

We have shown the dependences of the optical absorption, the ground state energy level, and the interfacial electron transfer dynamics on the size of CdSe QDs adsorbed on the (001), (110), and (111) surfaces of single crystal rutile-TiO_2 (R-TiO_2). The exponential optical absorption tail indicates a decrease in structural disorder or a decrease in the electron-phonon interactions with increasing size. The ground state energy levels of the CdSe QDs on (001) and (111) R-TiO_2 surfaces indicate an upward shift with increasing size, while that for the (110) surface shows a downward shift. These results suggest that the pinning of the CdSe QD ground state to the VBM depends on the orientation of the R-TiO_2. The excited state energy levels of CdSe QDs on (001), (110), and (111) R-TiO_2 surfaces indicate a downward shift with increasing size. The IET rate constant decreases with increasing size and depends on the R-TiO_2 surface orientation, indicating a decrease in the free energy change. The relative value of the parameter for the slow relaxation process increases with increasing size and depends on the R-TiO_2 surface orientation, indicating differences between the density of states in the conduction bands for (001), (110) and (111) single crystal R-TiO_2. The product of the IET rate constant and the relative value of the parameter for the slow relaxation process is related to the short circuit current density in QDSCs. The higher value of this product for CdSe QDs with a diameter of ~ 6.6 nm adsorbed on a (111) R-TiO_2 nanosheet is advantageous and can contribute to improvements in the photovoltaic performance of CdSe QDSCs.

AUTHOR INFORMATION

Corresponding Authors

*E-mail: toyoda@pc.uec.ac.jp (T. T.); Tel.: +81-42-443-5464

*E-mail: shen@pc.uec.ac.jp (Q. S.); Tel. +81-42-443-5471

Notes

The authors declare no competing financial interest.

ACKNOWLEDGMENTS

Part of this work was supported by Core Research for Evolutional Science and Technology (CREST), Japan Science Technology Agency (JST). The work was also supported by JSPS Kakenhi Grant Number 26390016. We thank T. Amano and Y. Takeshita (Bunkoukeiki Co., Ltd.) for cooperation with the photoelectron yield spectroscopy measurements.

REFERENCES

(1) Tongying, P.; Plashnista, V. V.; Petchsang, N.; Vietmeyer, F.; Ferraudi, G. J.; Krylova, G.; Kuno, M. Photocatalytic Hydrogen Generation Efficiencies in One-Dimensional CdSe Heterostructures. *J. Phys. Chem. Lett.* **2012**, *3*, 3234-3240.

(2) Kolny-Olesiak, J.; Weller, H. Synthesis and Application of Colloidal $CuInS_2$ Semiconductor Nanocrystals. *ACS Appl. Mater. Interfaces* **2013**, *5*, 12221-12237.

(3) Weng, B.; Liu, S. Q.; Tang, Z. R.; Xu, Y. J. One-Dimensional Nanostructure Based Materials for Versatile Photocatalytic Applications. *RSC Adv.* **2014**, *4*, 12685-12700.

(4) Simon, T.; Bouchonville, N.; Berr, M. J.; Vaneski, A.; Adrovic, A.; Volbers, D.; Wyrwich, R.; Döblinger, M.; Susha, A. S.; Rogach, A. L.; Jäckell, F.; Stolarczyk, J. K.; Feldmann, J. Redox Shuttle Mechanism Enhances Photocatalytic H_2 Generation on Ni-Decorated CdS Nanorods. *Nat. Mater.* **2014**, *13*, 1043-1018.

(5) Niitsoo, O.; Sarkar, S. K.; Pejoux, C.; Rühle, S.; Cahen, D.; Hodes, G. Chemical Bath Deposited CdS/CdSe-Sensitized Porous TiO_2 Solar Cells. *J. Photochem. Photobiol. A: Chemistry* **2006**, *181*, 306-313.

(6) Diguna, L. J.; Shen, Q.; Sato, A.; Katayama, K.; Sawada, T.; Toyoda, T. Optical Absorption and Ultrafast Carrier Dynamics Characterization of CdSe Quantum Dots Deposited on Different Morphologies of Nanostructured TiO_2 Films. *Mater. Sci. Eng. C* **2007**, *27*, 1514-1520.

(7) Diguna, L. J.; Shen, Q.; Kobayashi, J.; Toyoda, T. High Efficiency of CdSe Quantum-Dot-Sensitized TiO_2 Inverse Opal Solar Cells. *Appl. Phys. Lett.* **2007**, *91*, 023116.

(8) Kongkanand, A.; Tvrdy, K.; Takechi, K.; Kuno, M.; Kamat, P. V. Quantum Dot Solar Cells. Tuning Photoresponse through Size and Shape Control of CdSe TiO_2 Architecture. *J. Am. Chem. Soc.* **2008**, *130*, 4007-4015.

(9) Mora-Seró, I.; Giménez, S.; Fabregat-Santiago, F.; Gómez, R.; Shen, Q.; Toyoda, T.; Bisquert, J. Recombination in Quantum Dot Sensitized Solar Cells. *Acc. Chem. Res.* **2009**, *42*, 1848-1857.

(10) Mora-Seró, I.; Bisquert, J. Breakthroughs in the Development of Semiconductor-Sensitized Solar Cells. *J. Phys. Chem. Lett.* **2010**, *1*, 3046-3052.

(11) Emin, S.; Singh, S. P.; Han, L.; Satoh, N.; Islam, A. Colloidal Quantum Dot Solar Cells. *Sol. Energy* **2011**, *85*, 1264-1282.

(12) Toyoda, T.; Shen, Q. Quantum-Dot-Sensitized Solar Cells: Effect of Nanostructured TiO_2 Morphologies on Photovoltaic Properties. *J. Phys. Chem. Lett.* **2012**, *3*, 1885-1893.

(13) Yindeesuk, W.; Shen, Q.; Hayase, S.; Toyoda, T. Optical Absorption of CdSe Quantum Dots on Electrodes with Different Morphology. *AIP Adv*. **2013**, *3*, 102115.

(14) Toyoda, T.; Onishi, Y.; Katayama, K.; Sawada, T.; Hayase, S.; Shen, Q. Photovoltaics and Photoexcited Carrier Dynamics of Double-Layered CdS/CdSe Quantum Dot-Sensitized Solar Cells. *J. Mater. Sci. Eng. A* **2013**, *3*, 601-608.

(15) Toyoda, T.; Yindeesuk, W.; Okuno, T.; Akimoto, M.; Kamiyama, K.; Hayase, S.; Shen, Q. Electronic Structures of Two Types of TiO_2 Electrodes: Inverse Opal and Nanoparticulate Cases. *RSC Adv.* **2015**, *5*, 49623-49632.

(16) Underwood, D. F.; Kippeny, T.; Rosenthal, S. J. Charge Carrier Dynamics in CdSe Nanocrystals: Implications for the Use of Quantum Dots in Novel Photovoltaics. *Eur. Phys. J. D* **2001**, *16*, 241-244.

(17) Salant, A.; Shalom, M.; Tachan, Z.; Buhbut, S.; Zaban, A.; Banin, U. Quantum Rod-Sensitized Solar Cell: Nanocrystal Shape Effect on the Photovoltaic Properties. *Nano Lett.* **2012**, *12*, 2095-2100.

(18) Yella, A.; Lee, H.-W.; Tsao, H. N.; Yi, C.; Chandiran, A. K.; Nazeeruddin, Md. K.; Wei-Guang Diau, E.; Yeh, C-Y.; Zakeeruddin, S. M.; Grätzel, M. Porphyrin-Sensitized Solar Cells with Cobalt (II/III)-Based Redox Electrolyte Exceed 12 Percent Efficiency. *Science* **2011**, *334*, 629-634.

(19) Tian, J.; Gao, G. Control of Nanostructures and Interfaces of Metal Oxide Semiconductors for Quantum-Dots-Sensitized Solar cells. *J. Phys. Chem. Lett.* **2015**, *6*, 1859-1689.

(20) Jin, S.; Lian T. Electron Transfer dynamics of Single Quantum Dots on the (110) Surface of a Rutile TiO_2 Single Crystal. *Sci. China Chem.* **2011**, *54*, 1898-1902.

(21) Diebold, U. The Surface of Titanium Dioxide. *Surf. Sci. Rep.* **2003**, *48*, 53-229.

(22) Etgar, L.; Zhang, W.; Gabriel, S.; Hickey, S.G.; Nazeerudin, Md. K.; Eychmüller, A.; Liu, B.; Grätzel, M. High Efficiency Quantum Dot Heterojunction Solar Cell Using Anatase (001) TiO_2 Nanosheets. *Adv. Mater*. **2012**, *24*, 2202-2206.

(23) Kavan, L.; Grätzel, M.; Gilbert, S. E.; Klemenz, C.; Scheel, H. J. Electrochemical and Photoelectrochemical Investigation of Single-Crystal Anatase. *J. Am. Chem. Soc.* **1996**, *118*, 6716-6723.

(24) Maitani, M. M.; Tanakai, K.; Mochizuki, D.; Wada, Y. Enhancement of Photoexcited Charge Transfer by {001} Facet-Dominating TiO_2 Nanoparticles. *J. Phys. Chem. Lett.* **2011**, *2*, 2655-2659.

(25) Takeda, N.; Parkinson, B. A. Adsorption Morphology, Light Absorption, and Sensitization Yields for Squaraine Dyes on SnS_2 Surfaces. *J. Am. Chem. Soc.* **2003**, *125*, 5559-5571.

(26) Ushiroda, D.; Ruzycki, N.; Lu Y.; Spitler, M. T.; Parkinson, B. A. Dye Sensitization of the Anatase (101) Crystal Surface by a Series of Dicarboxylated Thiacyanine Dyes. *J. Am. Chem. Soc.* **2005**, *127*, 5158-5168.

(27) Sambur, J. B.; Parkinson, B. A. CdSe/ZnS Core/Shell Quantum Dot Sensitization of Low Index TiO_2 Single Crystal Surfaces. *J. Am. Chem. Soc.* **2010**, *132*, 2130-2131.

(28) Sambur, J. B.; Averill, C. M.; Bradly, C.; Schuttlefield, J.; Lee, S. H.; Reynolds, J. R.; Schanze, K. S.; Parkinson, B. A. Interfacial Morphology and Photoelectrochemistry of Conjugated Polyelectrolysis Adsorbed on Single Crystal TiO_2. *Langmuir* **2011**, *27*, 11906-11916.

(29) Sambur, J. B.; Parkinson, B. A. Size Selective Photoetching of CdSe Quantum Dot Sensitization on Single-Crystal TiO_2. *ACS Appl. Mater. Interfaces* **2014**, *6*, 21916-21920.

(30) Liang, Y.; Novet, T.; Thorne, J. E.; Parkinson, B. A. Photosensitization of ZnO Single Crystal Electrodes with PbS Quantum Dots. *Phys. Status Solidi A* **2014**, *211*, 1954-1959.

(31) Liang, Y.; Thorne, J. E.; Kern, M. E.; Parkinson, B. A. Sensitization of ZnO Single Crystal Electrodes with CdSe Quantum Dots. *Langmuir* **2014**, *30*, 12551-12558.

(32) Watkins, K. J.; Parkinson, B. A.; Spitler, M. T. Physical Models for Charge Transfer at Single Crystal Oxide Semiconductor Surfaces as Revealed by the Doping Density Dependence of the Collection Efficiency of Dye Sensitized Photocurrents. *J. Phys. Chem. B* **2015**, *119*, 7579-7588.

(33) Anderson, N. A.; Lian, T. Ultrafast Electron Transfer at the Molecule-Semiconductor Nanoparticle Interface. *Ann. Rev. Phys. Chem.* **2005**, *56*, 491-519.

(34) Huang, J.; Stockwell, D.; Boulesbaa, A.; Guo, J.; Lian, T. Comparison of Electron Injection Dynamics from Rhodamine B to In_2O_3, SnO_2, and ZnO Nanocrystalline Thin Films. *J. Phys. Chem. C* **2008**, *112*, 5203-5212.

(35) Jin, S.; Lian, T. Electron Transfer Dynamics from Single CdSe/ZnS Quantum Dots to TiO_2 Nanoparticles. *Nano Lett.* **2009**, *9*, 2448-2454.

(36) Stockwell, D.; Yang, Y.; Huang, J.; Anfuso, C.; Huang, Z.; Lian, T. Comparison of Electron-Transfer Dynamics from Coumarin 343 to TiO_2, SnO_2, and ZnO Nanocrystalline Thin Films: Role of Interface-Bound Charge-Separated Pairs. *J. Phys. Chem. C* **2010**, *114*, 6560-6566.

(37) Tvrdy, K.; Frantsuzov, P. A.; Kamat, P. V. Photoinduced Electron Transfer from Semiconductor Quantum Dots to Metal Oxide Nanoparticles, *Proc. Natl. Acad. Sci. U. S. A.* **2011**, *108*, 29-34.

(38) Zheng, K.; Žídek, K.; Abdelah, M.; Chábera, P.; Abd El-sadek, M. S.; Pullerits, T. Effect of Metal Oxide Morphology on Electron Injection from CdSe Quantum Dots to ZnO. *Appl. Phys. Lett.* **2013**, *102*, 163119.

(39) Zheng, K.; Žídek, K.; Abdelah, M.; Zhang, W.; Chábera, P.; Lenngren, N.; Yartsev, A.; Pullerits, T. Ultrafast Charge Transfer from CdSe Quantum Dots to p-Type NiO: Hole Injection vs Hole Trapping. *J. Phys. Chem. C* **2014**, *118*, 18462-18471.

(40) Abdellah, M.; Marschan, R.; Žídek, K.; Messing, M. E.; Abdelwahab, A.; Chábera, P.; Zheng, K.; Pullerits, T. Hole Trapping: The Critical Factor for Quantum Dot Sensitized Solar Cell Performance. *J. Phys. Chem. C* **2014**, *118*, 25802-25808.

(41) Hansen, T.; Žídek, K.; Zheng, K.; Abdellah, M.; Chábera, P.; Persson, P.; Pullerits, T. Optical Topology Controlling Charge Injection in Quantum-Dot-Sensitized Solar Cells. *J. Phys. Chem. Lett.* **2014**, *5*, 1157-1162.

(42) Zheng, K.; Karki, K.; Žídek, K.; Pullerits, T. Ultrafast Photoinduced Dynamics in Quantum Dot-Based Systems for Light Harvesting. *Nano Res.* **2015**, *8*, 2125-2142.

(43) Toyoda, T.; Yindeesuk, W.; Kamiyama, K.; Katayama, K.; Kobayashi, H.; Hayase, S.; Shen, Q. The Electronic Structure and Photoinduced Electron Transfer Rate of CdSe Quantum Dots on Single Crystal Rutile TiO_2: Dependence on the Crystal Orientation of the Substrate. *J. Phys. Chem. C* **2016**, *120*, 2047-2057.

(44) Toyoda, T.; Tsugawa, S.; Shen, Q. Photoacoustic Spectra of Au Quantum Dots Adsorbed on Nanostructured TiO_2 Electrodes Together with the Photoelectrochemical Current Characteristics. *J. Appl. Phys.* **2009**, *105*, 034314.

(45) Toyoda, T.; Oshikane, K.; Li, D.; Luo, Y.; Meng, Q.; Shen, Q. Photoacoustic and Photoelectrochemical Current spectra of Combined CdS/CdSe Quantum Dots Adsorbed on Nanostructured TiO_2 Electrodes, together with Photovoltaic Characteristics. *J. Appl. Phys.* **2010**, *108*, 114304.

(46) Honda, M.; Kanai, K.; Komatsu, K.; Ouchi, Y.; Ishii, H.; Seki, K. Atmospheric Effect of Air, N_2, and Water Vapor on the Ionozation Energy of Titanyl Phthalocyanine Thin Film Studies by Photoemission Yield Spectroscopy. *J. Appl. Phys.* **2007**, *102*, 103704.

(47) Nakayama, Y.; Machida, S.; Minari, T.; Tsukagishi, K.; Noguchi, Y.; Ishii, H. Direct Observations of the Electronic State of Single Crystalline Rubrene under Ambient Condition by Photoelectron Yield Spectroscopy. *Appl. Phys. Lett.* **2008**, *93*, 173305.

(48) Katayama, K.; Yamaguchi, M.; Sawada, T. Lens-Free Heterodyne Detection for Transieint Grating Experiments. *Appl. Phys. Lett.* **2003**, *82*, 2775-2777.

(49) Shen, Q.; Katayama, K.; Sawada, T.; Toyoda, T. Characterization of Electron Transfer from CdSe Quantum Dots to Nanostructured TiO_2 Electrode Using a Near-Field Heterodyne Transient Grating Technique. *Thin Solid Films* **2008**, *516*, 5927-5930.

(50) Toyoda, T.; Yindeesuk, W.; Kamiyama, K.; Hayase, S.; Shen, Q. Effect of TiO_2 Crystal Orientation on the Adsorption of CdSe Quantum Dots for Photosensitization Studied by the Photoacoustic and Photoelectron Yield Methods. *J. Phys. Chem. C* **2014**, *118*, 16680-16687.

(51) Mazumdar, S.; Roy, K.; Srihari, V.; Umapathy, S.; Bhattacharyya, A. J. Probing Ultrafast Photoinduced Electron Transfer to TiO_2 from CdS Nanocrystals of Varying Crystallographic Phase Content. *J. Phys. Chem. C* **2015**, *119*, 17466-17473.

(52) Rosencwaig, A.; Gersho, A. Theory of the Photoacoustic Effect with Solids. *J. Appl. Phys.* **1976**, *47*, 64-69.

(53) Ballantyne, J. M. Effect of Photon Energy Loss on Photoemissive Yield near Threshold. *Phys. Rev. B* **1972**, *6*, 1436.

(54) Rosencwaig, A. Photoacoustic Spectroscopy – A New Tool for Investigation of Solids. *Anal. Chem.* **1975**, *47*, 592A-604A.

(55) Ekimov, A. I.; Efros, Al. L.; Onushchenko, A.A. Quantum Size Effect in Semiconductor Microcrystals. *Solid State Commun.* **1985**, *56*, 921-924.

(56) Murray, C. B.; Norris, D. J.; Bawendy, M. G. Synthesis and Characterization of Nearly Monodisperse CdE (E = S, Se, Te) Semiconductor Nanocrystallites. *J. Am Chem. Soc.* **1993**, *115*, 8706-8715.

(57) Urbach, F. The Long-Wavelength Edge of Photographic Sensitivity and of the Electronic Absorption of Solids. *Phys. Rev.* **1953**, *92*, 1324.

(58) Meeder, A.; Fuertes Marrón, D.; Rumberg, A.; Lux-Steiner, M. Ch.; Chu, V.; Conde, J. P. Direct Measurement of Urbach Tail and Gap State Absorption in CuGaSe2 Thin Films by Photothermal Deflection Spectroscopy and the Constant Photocurrent Method. *J. Appl. Phys.* **2002**, *92*, 3016-3020.

(59) Wasim, S. M.; Rincón, C.; Marín, G.; Bocaranda, P. Effect of Structural Disorder on the Urbach Energy in Cu Ternaries. *Phys. Rev. B* **2001**, *64*, 195101.

(60) Jones, D. A.; Ung Lee, J. Observation of the Urbach Tail in the Effective Density of States in Carbon Nanotubes. *Nano Lett.* **2011**, *11*, 4176-4179.

(61) Hachiya, S.; Shen, Q.; Toyoda, T. Effect of ZnS Coatings on the Enhancement of the Photovoltaic Properties of PbS Quantum Dot-Sensitized Solar Cells. *J. Appl. Phys.* **2012**, *111*, 104315.

(62) Rai, R. C. Analysis of the Urbach Tails in Absorption Spectra of Undoped ZnO Thin Films. *J. Appl. Phys.*, **2013**, *113*, 153508.

(63) De Wolf, S.; Holovsky, J.; Moon, S-J.; Löper, P.; Niesen, B.; Ledinsky, M.; Haug, F-J.; Yum, J-H.; Ballif, C. Organometallic Halide Perovskites: Sharp Optical Absorption Edge and Its Relation to Photovoltaic Performance. *J. Phys. Chem. Lett.* **2014**, *5*, 1035-1039.

(64) Toyoda, T.; Yindeesuk, W.; Kamiyama, K.; Hayase, S.; Shen, Q. Adsorption and Electronic Structure of CdSe Quantum Dots on Single Crystal ZnO: A Basic Study of Quantum Dot-Sensitization System. *J. Phys. Chem. C* **2016**, *120*, 16367-16376.

(65) Brus, L. B. Electronic Wave Functions in Semiconductor Clusters: Experiment and Theory. *J. Phys. Chem.* **1986**, *90*, 2555-2560.

(66) Carlson, B.; Leschkies, K.; Aydal, E. S.; Zhu, X.-Y. Valence band Alignment at Cadmium Selenide Quantum Dot and Zinc Oxide (10$\bar{1}$0) Interfaces. *J. Phys. Chem. C* **2008**, *112*, 8419-8423.

(67) Guijarro, N.; Lana-Villarreal, T.; Shen, Q.; Toyoda, T.; Gómez, R. Sensitization of Titanium Dioxides with Cadmium Selenide Quantum Dots Prepared by SILAR: Photoelectrochemical and Carrier Dynamics Studies. *J. Phys. Chem. C* **2010**, *114*, 21928-21937.

(68) Guijarro, N.; Shen, Q.; Giménez, S.; Mora-Seró, I.; Bisquert, J.; Lana-Villarreal, T.; Toyoda, T.; Gómez, R. Direct Correlation between Ultrafast Injection and Photoanode Performance in Quantum Dot Sensitized Solar Cells. *J. Phys. Chem. C* **2010**, *114*, 22352-22360.

(69) Pernik, D. R.; Tvrdy, K.; Radich, J. G.; Kamat, P. V. Tracking the Adsorption and Electron Injection Rates of CdSe Quantum Dots on TiO_2: Linked versus Direct Attachment. *J. Phys. Chem. C* **2011**, *115*, 13511-13519.

(70) Akimov, A. V.; Neukirch, a. J.; Prezhdo, O. V. Theoretical Insights into Photoinduced Charge Transfer and Catalysis at Oxide Interfaces. *Chem. Rev.* **2013**, *113*, 4496-4565.

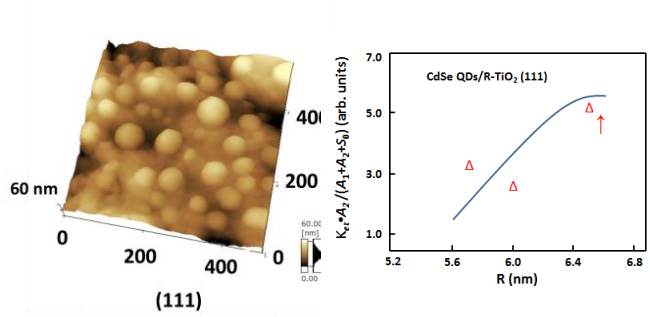
60 nm
0
200
400
0
200
400
(111)
CdSe QDs/R-TiO2 (111)
Kex*A2/(A1+A2+S0) (arb. units)
7.0
5.0
3.0
1.0
5.2
5.6
6.0
6.4
6.8
R (nm)

TOC Image